An Extrasolar Planet Transit Search with Subaru Suprime-Cam

Uragawa, Seitaro ; Yamada, Toru ; Suto, Yasushi ; Edwin L. Turner ;
Itoh, Yoichi ; Mukai, Tadashi ; Tamura, Motohide ; Yiping Wang

An Extrasolar Planet Transit Search with Subaru Suprime-Cam[*]

Seitaro URAKAWA,[1,5] Toru YAMADA,[2] Yasushi SUTO,[3] Edwin L. TURNER,[4]

Yoichi ITOH,[5] Tadashi MUKAI,[5] Motohide TAMURA,[2] and Yiping WANG[6]

[1]*Bisei Spaceguard Center, 1716-3 Okura, Bisei-cho, Ibara, Okayama 714-1411*
urakawa@spaceguard.or.jp

[2]*National Astronomical Observatory of Japan, 2-21-1 Osawa, Mitaka, Tokyo 181-8588*
yamada@optik.mtk.nao.ac.jp, hide@optik.mtk.nao.ac.jp

[3]*Department of Physics, School of Science, The University of Tokyo, Hongo, Bunkyo-ku, Tokyo 113-0033*
suto@utap.phys.s.u-tokyo.ac.jp

[4]*Princeton University Observatory, Peyton Hall, Princeton, NJ 08544, USA*
elt@astro.princeton.edu

[5]*Graduate School of Science and Technology, Kobe University, 1-1 Rokkodai-cho, Nada-ku, Kobe 657-8501*
yitoh@kobe-u.ac.jp, mukai@kobe-u.ac.jp

[6]*Purple Mountain Observatory, Chinese Academy of Sciences, Nanjing 210008, China*
ypwang@pmo.ac.cn

(Received 2006 February 25; accepted 2006 July 5)

Abstract

We report the results of a prototype photometric search for transiting extrasolar planets using Subaru Suprime-Cam. Out of about 100000 stars monitored around the Galactic plane ($l = 90°$, $b = 0°$), we find that 7700 show photometric precision better than 1% for 60 s exposures, which is required to detect extrasolar planets by the transit method. Thus, Suprime-Cam has the photometric stability and accuracy necessary for a transiting planet survey. During this observing run, we detected three objects (around 18.5 mag for i'-band) that exhibit a single full transit-like light curve with a fractional depth of $< 5\%$. While a spectroscopic follow-up remains to be done using future telescopes in the 20–30 m class, the estimated parameters for the three systems are consistent with the planetary size companions around main-sequence stars. We also found two eclipsing binary candidates and eleven variable stars exhibiting W UMa-like light curves.

Key words: stars: binaries: eclipsing — stars: planetary systems — techniques: photometric

1. Introduction

Since the first discovery in 1995 (Mayor, Queloz 1995), more than 190 extrasolar planets around main-sequence stars have been reported so far. While a majority of them were discovered by the radial-velocity method, the transit method, i.e., detecting a small decrement in stellar light due to occultation by planets, provides a unique complementary means to estimate the precise radius and orbital inclination of those planets that exhibit transit. Combined with the radial-velocity data, the absolute mass, the semi-major axis, the orbital period, and the mean density of the transiting planets are determined. The transit method is particularly suited for detecting "very hot Jupiters" (gas giant planets with an orbital period in the range of $1\,\mathrm{d} \leq P \leq 3\,\mathrm{d}$) and "hot Jupiters" ($3\,\mathrm{d} < P \leq 9\,\mathrm{d}$) (Gaudi et al. 2005).

The difficulties for the transit method are as follows: there are numerous false positives arising from multiple systems; follow-up observations are difficult with the radial-velocity method; the geometrical probability of a transit is small; and the photometric accuracy required to detect the typical transit depth ($\sim 1\%$) is demanding. These imply that wide-field accurate photometric monitoring is necessary for successful detection of planets using the transiting method. This is why only seven extrasolar planets have been discovered first by the transit method, and then confirmed by a subsequent follow-up by radial velocity measurements [3 additional transiting planets (Charbonneau et al. 2000; Sato et al. 2005; Bouchy et al. 2005a) were discovered first by the radial velocity method, and their photometric transit signatures were found later]. Five out of the seven confirmed transiting planets were discovered by the Optical Gravitational Lensing Experiment (OGLE) survey (Udalski et al. 2002a, 2002b, 2002c, 2003, 2004). Indeed, they reported more than 130 extrasolar planet candidates that were observed with a high photometric precision of 0.015 mag or better. Follow-up observations using the radial-velocity method have so far confirmed three very hot Jupiters and two hot Jupiters from the candidates (Bouchy et al. 2004, 2005b; Dreizler et al. 2002; Konacki et al. 2003a, 2003b, 2004, 2005; Moutou et al. 2004; Pont et al. 2004; Torres et al. 2004, 2005). The remaining transiting planets were discovered by the Trans-Atlantic Exoplanet Survey network (TrEs) and the XO Project using wide-field CCD telescopes on small-aperture systems (Alonso et al. 2004; McCullough et al. 2005).

A number of transit search programs are currently on-going: the Extrasolar Planet Occultation Research (EXPLORE) project

---

[*] Based on data collected at the Subaru Telescope, which is operated by the National Astronomical Observatory of Japan.

(Mallén-Ornelas et al. 2003) conducts deep transit searches of the Galactic plane using the MOSAIC II camera at the CTIO 4 m telescope and the CFH12K camera at the 3.6 m Canada-France-Hawaii Telescope. The MOA-I project observed 14 Galactic Bulge fields using the 61 cm Boller and Chivens Telescope at Mt John University Observatory with three 2048×4096 pixels CCDs (Abe et al. 2005). Hood et al. (2005) observed NGC 6940 using the 2.5 m Isaac Newton Telescope with its Wide Field Camera, a mosaic consisting of four 2048×4096 pixels CCDs. Other cluster surveys — EXPLORE/OC (von Braun et al. 2005), PISCES (Mochejska et al. 2005, 2006), and STEPSS (Burke et al. 2006) — are also on-going. SuperWASP (Christian et al. 2004), Vulcan (Borucki et al. 2001), BEST (Rauer et al. 2004), HAT (Bakos et al. 2004), KELT (Pepper et al. 2004), and PASS (Deeg et al. 2004) are also conducting very wide-field transit surveys similar to TrEs and XO. While transiting planet candidates have been reported by these programs, the existence of the planets has not yet been confirmed.

Transit search space missions are also planned, including COROT (French Space Agency CNES, with participation of Austria, Belgium, Brazil, Germany, Spain, ESP, and ESTEC) and KEPLER (NASA). These missions are expected to achieve a photometric precision on the order of 0.01%, and aim to detect terrestrial planets in the habitable zone of their primary stars by the photometric transit method (Bordé et al. 2003; Basri et al. 2005).

In this paper, we describe a prototype transit search using Subaru Suprime-Cam carried out in 2002. While our observing run covered only a small range in the time domain (15 observing hours in total over 4 consecutive nights), the field-of-view was significantly wider ($34' \times 27'$), and the survey magnitude was deeper than those of OGLE, EXPLORE and MOA-I. Thus, we mainly looked for single transit events, and performed a serious attempt to test the feasibility of the photometric transiting planet search using Subaru Suprime-Cam for the first time.

The rest of the paper is organized as follows: section 2 describes our observational strategies and data-reduction procedures. In section 3, we discuss the achieved photometric precision. Section 4 presents candidate transiting objects; we found three single-transit objects and two double-transit objects (possibly eclipsing binaries). Assuming circular orbits, we estimate the radii and the orbital elements of the companions. Finally, section 5 is devoted to a summary. We also discovered eleven W UMa-like eclipsing binary systems, which are reported in the Appendix.

2. Observations and Data Reduction

2.1. Transit Search

In order to maximize the number of available stars, we selected a region of $34' \times 27'$ at the Galactic plane centered at $l = 90°$, $b = 0°$ for our photometric survey. The field was imaged with Suprime-Cam on the 8.2 m Subaru Telescope, which consists of 5×2 CCD chips with 2024×4048 pixels each. Thus, the detector scale corresponds to $0.''202$ per pixel. We repeated photometric observations of the field with 60 s exposures and read-out times of 60 s each for 6 hr on 2002 September 28 and 29 and for 1.5 hr on 2002 October 1 and 2.

The fractional transit depth, ΔF, is expressed as

$$\Delta F = \left(\frac{R_\mathrm{p}}{R_*} \right)^2, \tag{1}$$

where R_p is the radius of a planet and R_* is the radius of a parent star; the depth is approximately 1% for a Jupiter-size planet orbiting around a Sun-like star. Equation (1) indicates that relatively small-size stars, such as late-type dwarfs, are better suited for transit detection. Since late-type dwarfs are brighter at longer wavelength, we chose i'-band for the transit photometry; the z'-band is expected to be seriously compromised by high sky noise. In order to avoid the effects of any systematic errors in flat fielding, we did not conduct dithering, and tried to observe stars at constant position on the CCD. We obtained 383 frames in the i'-band for the entire observing run. Excluding seven frames that suffered from telescope tracking errors, we used 376 images to search for transit events. The sky was clear on September 28 and October 1 and 2, but on September 29 there were occasionally thin clouds. The seeing was approximately $0.''5–0.''8$ during the observing runs. We used GD 248 as a standard star (Oke 1990) to determine the zero point of the i'-band photometry.

Bias was estimated from the overscan region and subtracted from each frame. When carrying out this standard procedure, we used the IRAF package[1] for i'-band images and the Suprime-Cam Deep Field REDuction (SDFRED) package (Yagi et al. 2002; Ouchi et al. 2004) for multicolor photometry. The dark current was completely negligible for 60 s exposures (Miyazaki et al. 2002). The median of normalized dome frames was used as the flat frame. An example of the reduced image of chip 2 for the i'-band is shown in figure 1. This image was obtained on September 29 and the field-of-view was 1/10 of the total (10 chips).

We carried out aperture photometry using the IRAF package. We selected a value of 10 pixels for the aperture radius (i.e., approximately 3 times of FWHM for the PSF). Those objects with their i'-band magnitudes satisfying $18 \leq i' \leq 23$ were analyzed; we excluded $i' \leq 18$ objects because of flux saturation, and $i' \geq 23$ objects because of insufficient counts for accurate photometry. The number of selected point sources exceeded 100000.

A change in the atmospheric airmass is the primary source of absolute fluctuation in the light curves. In order to determine the atmospheric change, we select more than 200 stars per CCD chip image as references. We calculated the weighted mean

---

[1]   IRAF is distributed by the National Optical Astronomy Observatories, which are operated by the Association of Universities for Research in Astronomy, Inc., under cooperative agreement with the National Science Foundation, USA.
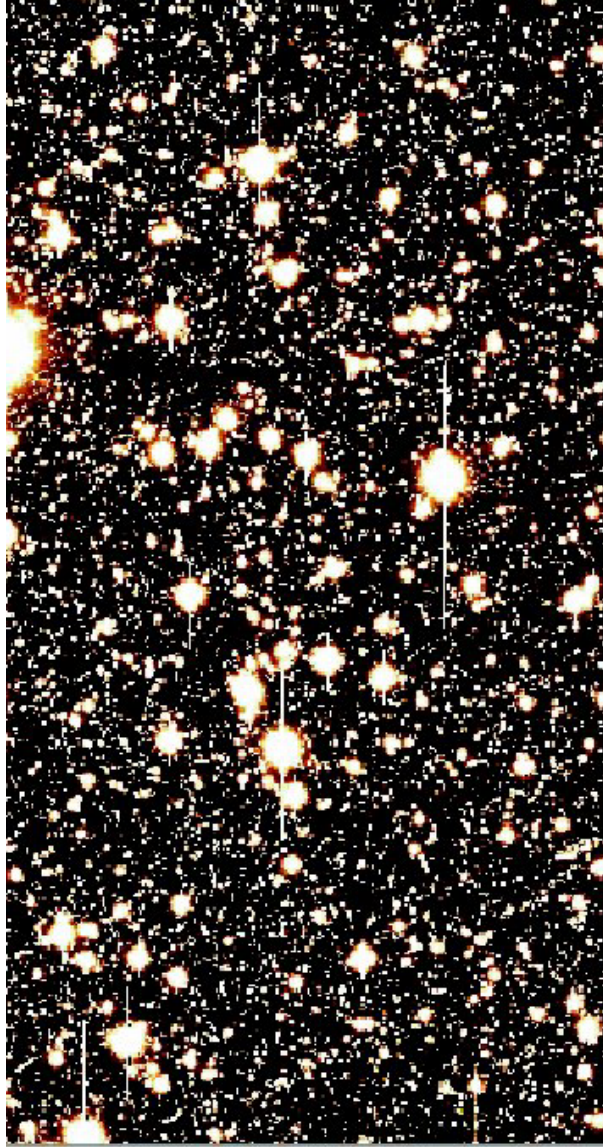
Fig. 1. Example of the reduced i'-band image for chip 2. The field of view of this image is approximately $7' \times 13'$. The entire field of view of Suprime-Cam consists of ten chips (each chip has 2048×4096 pixels), and is thus ten-times as large as this image. The entire observed region is centered at the Galactic plane of $l = 90°$, $b = 0°$.

fluxes of these reference stars weighted by the flux error, which were represented by Poisson noise and sky noise for each star. While short-period variable stars might be included in the reference stars, they are very rare and their contribution is expected to be negligible; the fractional ratio of W UMa-like eclipsing variables, whose periods typically range between 0.2 and 1.0 d, is approximately one in 250–300 main sequences. After correcting for the atmospheric airmass and transparency, we computed the fluxes of each star for every frame, and defined the photometric precision for each star as the standard deviation among all the frames on September 28 and 29. More specifically the photometric precision is given as

$$\sigma = \sqrt{\frac{1}{n}\sum_{i=1}^{n}(F_i - \overline{F})^2}. \tag{2}$$

Here, σ is the photometric precision and n is the number of frames for each night; F_i and $\overline{F}$ are the calibrated flux of each star for every frame and the mean flux of each star for every night, respectively.
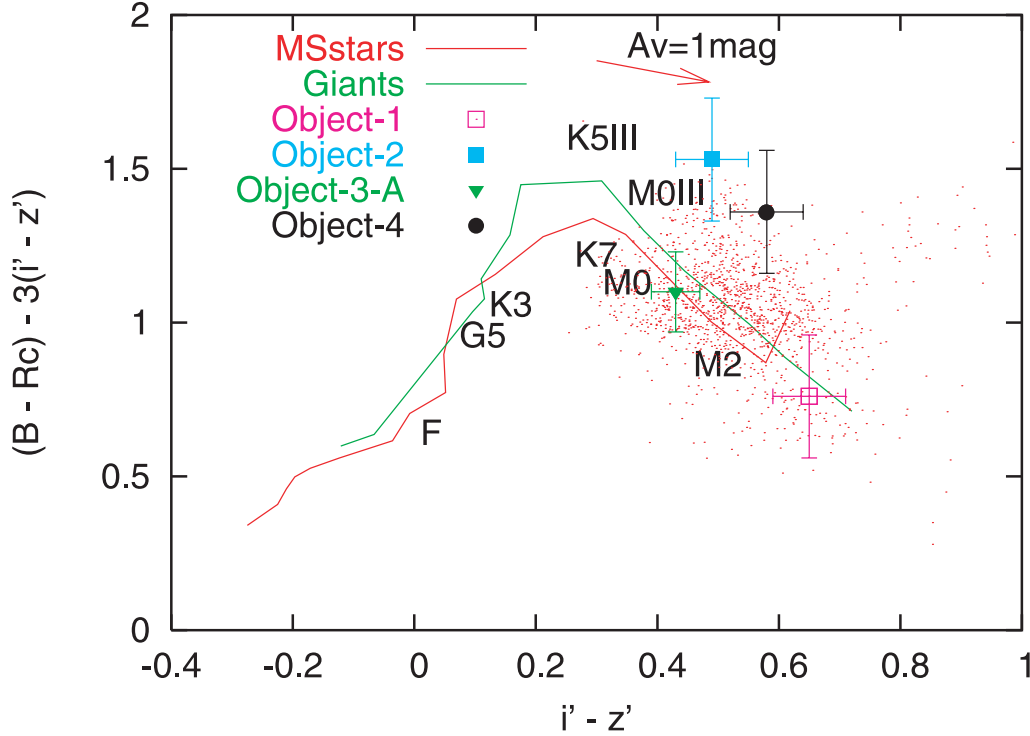
Fig. 2. Color–color diagram for objects on chip 4 and transiting candidates discussed in section 4. We plot only good photometry objects whose magnitude error is less than 0.055 mag and 0.2 mag for $i' - z'$ and $B - R_c - 3(i' - z')$, respectively. The red and green lines indicate the positions of the unreddened main sequences and giants, respectively (Bessell 1990; Fukugita et al. 1996). The arrow represents the reddening vector.
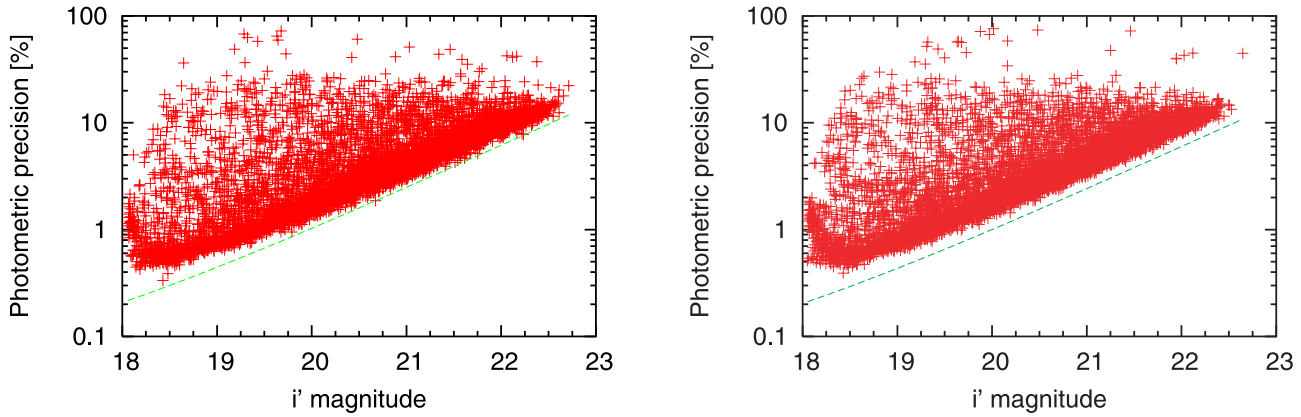
Fig. 3. Magnitude vs. photometric precision for objects detected in chip 2 on September 28 (*Left*) and September 29 (*Right*).

2.2. Multicolor Photometry

We conducted multicolor photometry in the B, R_c, and z' bands to determine the spectral types of the stars. We obtained one image in each band. We did not observe reference stars for these bands (except for i'). Instead, we used the mean flux of the reference stars in the Subaru/XMM-Newton Deep Survey field (SXDS-field) observed on the same nights as our observing run in order to determine the zero point in the B, R_c, and z' bands. From the inferred spectral type of each star, we estimated its radius and mass approximately. Moreover, we inferred the distance of objects from their the apparent magnitude, corrected for reddening, and the typical absolute magnitude for the spectral type.

Figure 2 shows a color–color diagram for the detected stars in chip 4 and our transiting candidates, presented in section 4. In the figure, the red and green lines correspond to the positions of the unreddened main sequence and giant stars, respectively. The arrow in figure 2 is the reddening vector. We set the y-axis as $B - R_c - 3(i' - z')$ in order to clarify the locations of different spectral types just for illustrative purposes. The identification of spectral type includes the uncertainty that comes from the

magnitude error in figure 2. The distance uncertainty of objects mainly depends on the wide range of the spectral type. Figure 2 indicates that most of the monitored stars are of FGKM types, but that it is difficult to infer their luminosity classes from the multicolor photometry alone.

3. Photometry

3.1. Photometric Precision

Figure 3 shows the photometric precision for each star (defined in subsection 2.1) on chip 2 as a function of its i'-band magnitude. We note that all ten CCD chips show similar photometric precisions. The green dotted curve indicates the theoretical lower bound, the Poisson noise of the stellar fluxes and the typical sky noise in the imaging data on September 28. Clearly, the photometric precision of most stars is close to the theoretical limit, and a photometric precision as small as 0.4% is achieved for stars of $i' \sim 18$ mag. Stars of $i' \leq 20$ mag lie significantly above a photometric precision of 10% due to the contamination of the brightness of close saturated stars.

Figure 3 also suggests that the photometric precision on September 29 is not better than that on September 28 due to the occasional thin clouds. Thus, since the influence of weather on September 29 was small, the photometric precision on September 29 was sufficient to detect extrasolar planets. Among more than 100000 stars within the field of view, 7700 objects had a photometric precision less than 1.0% for each 60 s exposure. Table 1 gives the resulting number of stars that achieved a given photometric precision. Gould et al. (2006) estimated that the ratio of main-sequence FGK stars which accompany very hot Jupiters is about 1 to 690. Because the geometrical probability of a transit is assumed to be 0.15, the ratio of transiting very hot Jupiter systems is about 1 to 4600.

In addition to simple issues of photometric precision, there are important systematic sources of error to consider. These include the likelihoods of false positives due to multiple star systems and of missing transits due to the limited duration of the observing run. The latter effect could easily decrease the detection probabilities by an additional factor of 3 or more. Thus, it is essential to survey a large number of stars in order to detect even a few transiting very hot Jupiters.

3.2. Selection of Candidates

Typical transit durations of the previously detected systems (Udalski et al. 2002a, 2002c; Alonso et al. 2004) are a few hours. Thus, we define transit candidates as light curves that have more than fifteen continuous data points (approximately 30 min per well-sampled light curve) that exhibit more than a 1σ flux decrement with respect to the average flux during an observing run. According to the selection criteria, we were left with around 1000 objects out of more than 100000 objects. We then inspected the light curves of all selected objects by eye. Independently, in order to detect periodic variable stars and double transit events, we conducted a period analysis using the phase dispersion minimization (PDM) algorithm described by Stellingwerf (1978). This algorithm minimizes scatter for a given data set phased to a series of test periods. The likelihood of a given test period is given by the parameter Θ. The minimum value for Θ represents the minimum dispersion of data points for a given period. We selected around 2000 objects with Θ less than 0.5, from more than 100000 objects, as candidates for double transit objects and variable stars. We considered objects with full double decrements in stellar light as double transit objects. However, the folded light curves for double transit objects did not cover the full phase. Next, we selected objects with sine-like light curves as W UMa eclipsing binary candidates. Although the periods of those eclipsing binary candidates were estimated by the PDM method, the true period might actually be commensurate with the estimated period. For this reason, the Lomb periodogram method (Lomb 1976; Press et al. 1992) was employed for W UMa eclipsing binary candidates. The spectral power obtained by this method gives the statistically most significant period. Finally, we determined the W UMa eclipsing binary candidates according to the following criteria: (1) the fluxes were not contaminated by nearby stars, (2) the objects were detected in all bands, and (3) the data points covered approximately the full phase.

3.3. Estimation of Orbital Elements

Detections of multiple photometric transit events and extensive radial velocity follow-up are required to accurately determine the orbital elements of a companion around a parent star. Approximate values, however, may be estimated even from the light curve of a single transit event, assuming that (1) M_* and R_* (M_* is the mass of the parent star and R_* is the radius of the parent star) are inferred from the spectral type (e.g., Cox 2000), (2) the companion has a circular orbit, and (3) the mass of the companion satisfies $M_p \ll M_*$ (see, e.g., Seager, Mallén-Ornelas 2003). Then, the orbital period, P, the semi-major axis, a, and the inclination with respect to the line of sight, i, can be explicitly written as

Table 1. Summary of statistics for mean photometric precision achieved in the September 28 and 29 runs.

Photometric precision	$\leq 5.0\%$	$\leq 3.0\%$	$\leq 2.0\%$	$\leq 1.5\%$	$\leq 1.0\%$	$\leq 0.5\%$
Number of stars	41000	27000	18000	13500	7700	1000

$$P = \frac{M_*}{R_*^3} \frac{G\pi}{32} \frac{(t_T^2 - t_F^2)^{3/2}}{(\Delta F)^{3/4}}, \tag{3}$$

$$a = \left(\frac{P^2 G M_*}{4\pi^2} \right)^{1/3}, \tag{4}$$

$$\cos i = \frac{R_*}{a} \left\{ \frac{(1 - \sqrt{\Delta F})^2 - [\sin^2(t_F \pi / P) / \sin^2(t_T \pi / P)](1 + \sqrt{\Delta F})^2}{1 - [\sin^2(t_F \pi / P) / \sin^2(t_T \pi / P)]} \right\}^{1/2}, \tag{5}$$

where G is the gravitational constant, and t_T and t_F denote the total transit duration and the "flat-bottom" duration, respectively.

We attempted to compute the orbital elements of OGLE and TrEs planets using the above equations. The results are given in table 2. We found that while the estimated periods are different from the actual ones by several hours, the semi-major axes and the inclinations agree within around 0.01 AU and a few degrees, respectively.

In order to derive the transit depth, the transit duration and the flat-bottom duration, we need a template light curve for the fit. For that purpose, we used the perturbation result derived by Ohta, Taruya, and Suto (2005). The template flux is given as

$$F = 1 - \frac{f(\gamma, \rho)}{\pi(1 - u_1/3 - u_2/6)}. \tag{6}$$

Here, u_1 and u_2 are limb darkening parameters and they are defined as

$$I(\mu)/I(0) = [1 - u_1(1 - \mu) - u_2(1 - \mu)^2]. \tag{7}$$

Here, μ is an angle between the star's radius vector and the line of sight. Moreover, $f(\gamma, \rho)$ is given as

$$f(\gamma, \rho) = \begin{cases} \pi\gamma^2 \left[1 - u_1 - u_2 \left(2 - \rho^2 - \frac{1}{2}\gamma^2 \right) + (u_1 + 2u_2) W_1 \right] & \rho < 1 - \gamma \\[2ex] \left(1 - u_1 - \frac{3}{2}u_2 \right) \left[\gamma^2 \cos^{-1}\left(\frac{\zeta}{\gamma} \right) + \sin^{-1} z_0 - \rho z_0 \right] & \\[1ex] \quad + \frac{1}{2}u_2\rho \left[(\rho + 2\zeta)\gamma^2 \cos^{-1}\left(\frac{\zeta}{\gamma} \right) - z_0(\rho\zeta + 2\gamma^2) \right] & \\[1ex] \quad + (u_1 + 2u_2) W_3 & 1 - \gamma < \rho < 1 + \gamma \\[2ex] 0 & \rho > 1 + \gamma, \end{cases} \tag{8}$$

where γ, ρ, η_p, z_0, and ζ are defined as

$$\gamma = R_p/R_*, \tag{9}$$

$$\rho = 1 + \eta_p = \frac{\sqrt{X_p^2 + Z_p^2}}{R_*}, \tag{10}$$

$$z_0 = \frac{\sqrt{(\gamma^2 - \eta_p^2)\left[(\eta_p + 2)^2 - \gamma^2\right]}}{2(1 + \eta_p)}, \tag{11}$$

Table 2. Orbital elements for extrasolar planets and their estimated orbital elements using equations (1) and (3)–(5).

Object	P (observed | estimated) [d]	a (observed | estimated) [AU]	i (observed | estimated) [°]	ΔF [%]	t_T [min]	t_F [min]
OGLE-TR-10b[*]	3.101386 | 2.3	0.04162 | 0.034	89.2 | 86	1.61	174	141
OGLE-TR-56b[†]	1.2119189 | 1.3	0.0225 | 0.024	81 | 81	1.32	113	71
OGLE-TR-111b[‡]	4.01610 | 3.8	0.047 | 0.044	86.5–90 | 88	1.46	164	124
OGLE-TR-113b[§]	1.43250 | 1.5	0.0228 | 0.023	85–90 | 87	2.10	114	82
OGLE-TR-132b[§]	1.68965 | 2.4	0.0306 | 0.039	78–90 | 84	0.70	165	125
TrES-1[‖]	3.030065 | 3.1	0.0393 | 0.039	88.5 | 89	1.69	154	116

[*] Konacki et al. (2005), [†] Torres et al. (2004), [‡] Pont et al. (2004), [§] Bouchy et al. (2004), [‖] Alonso et al. (2004).
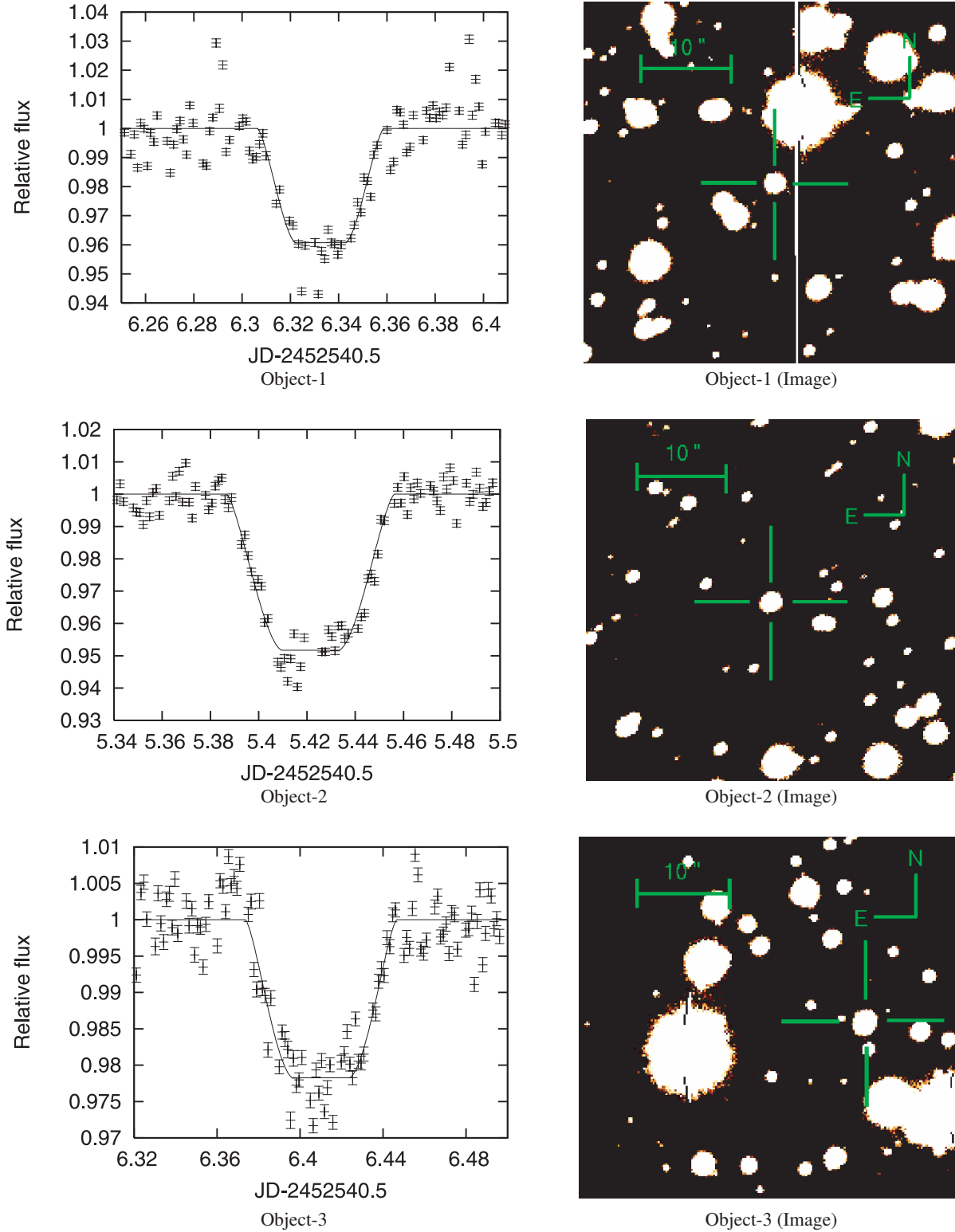
Fig. 4. *Left*: Light curves for the single transiting candidates. The best-fit light curve models are based on Ohta, Taruya, and Suto (2005). We assume a K0 dwarf radius for Object-1 and Object-3, and a K5 dwarf radius for Object-2. *Right*: Images for the single transiting candidates. Object-3 turns out to be a double star.
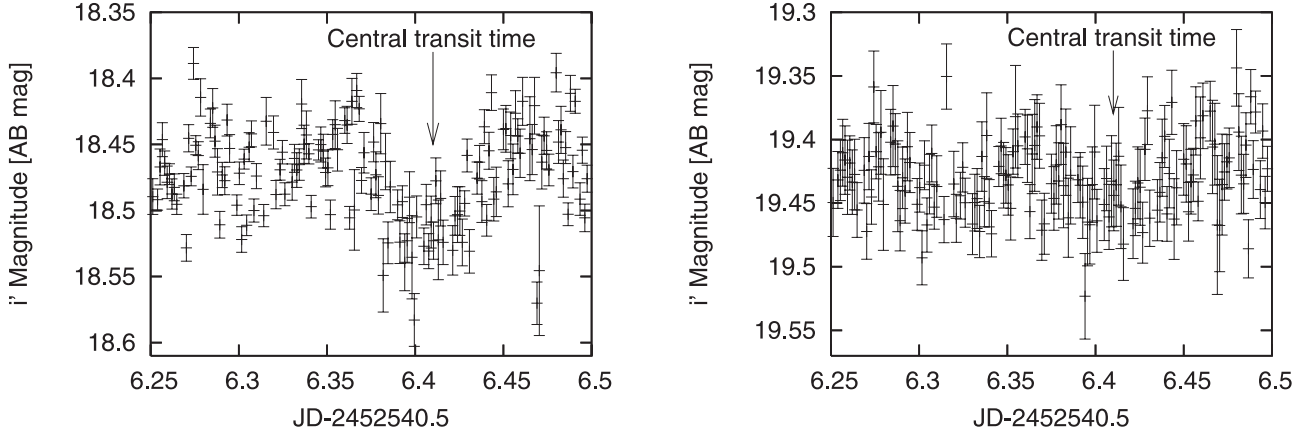
Fig. 5. Light curves of Object-3-A (*Left*) and Object-3-B (*Right*) from the PSF photometry. The arrow indicates the central transit time estimated from figure 4.

$$\zeta = \frac{2\eta_{\mathrm{p}} + \gamma^2 + \eta_{\mathrm{p}}^2}{2(1 + \eta_{\mathrm{p}})}. \tag{12}$$

Here, X_{p} and Z_{p} are the positions of the center of the planet in the star's central coordinate system. W_1 and W_3 are integrals that are defined in the Appendix of Ohta, Taruya, and Suto (2005). The shape of the template light curve depends on the orbital elements, the parent star radius, the planet radius and the limb darkening. In order to make the template light curve, we substituted the temporary orbital elements and the planet radius as free parameters. Since the parent star radius can be inferred from the spectral type, we used the typical stellar radius that corresponds to the spectral type instead of the free parameter. For the sake of simplicity, we did not consider the effect of limb darkening ($u_1 = u_2 = 0$). After the fit, we obtained the orbital elements by assigning the values of ΔF, t_{F}, and t_{T} into equations (1) and (3)–(5). The obtained orbital elements are not remarkably different from those of template light curve.

4. Candidate Transiting Objects

After visual inspection of around 1000 objects which satisfied our selection criteria, we found five transiting candidates: three objects (Object-1, Object-2, and Object-3-A) exhibit a single full transit-like event. Their fractional flux decrements ($\sim 5\%$) for a couple of hours are consistent with a planetary size transit. The other two objects (Object-4 and Object-5) show double transit events, and their transit depths indicate that they are binary star systems. Further information on those candidates is summarized in tables 3 and 4, and their light curves are shown in figures 4–6. The error of ΔF quoted in table 4 corresponds to the standard deviation for the model light curve. We briefly discuss each object below.

4.1. Object 1

Multicolor photometry indicates that Object-1 ($i' = 18.34$ AB mag) is either a G0/K5 or an M0/M5 star. It is likely that Object-1 is a dwarf because its distance exceeds the Galaxy scale ($> 17\,\mathrm{kpc}$) if it is a giant. Adopting typical parameters for a G0/K5 or M0/M5 dwarf, we estimated the companion size and orbital elements using equations (1) and (3)–(5), which are summarized in table 4.

Depending on the choice of the spectral type, and therefore the adopted radius, of the parent star, the companion takes two different sets of parameters. If it is an M dwarf and A_V is derived from its observed color and an unreddened standard M2 dwarf,

Table 3. Observed parameters for the transiting candidates.

Object	RA	Dec	B [mag]	R_{c} [mag]	i' [AB mag]	z' [AB mag]
Object-1	$21^{\mathrm{h}}13^{\mathrm{m}}35\overset{\mathrm{s}}{.}7$	$48°15'20\!''\!.6$	21.55 ± 0.02	18.84 ± 0.04	18.34 ± 0.05	17.69 ± 0.04
Object-2	$21^{\mathrm{h}}13^{\mathrm{m}}37\overset{\mathrm{s}}{.}2$	$48°10'37\!''\!.8$	22.04 ± 0.02	19.04 ± 0.03	18.50 ± 0.05	18.01 ± 0.04
Object-3-A	$21^{\mathrm{h}}11^{\mathrm{m}}42\overset{\mathrm{s}}{.}5$	$48° \ 9'46\!''\!.4$	21.13 ± 0.02	18.74 ± 0.02	18.47 ± 0.03	18.04 ± 0.03
Object-3-B	$21^{\mathrm{h}}11^{\mathrm{m}}42\overset{\mathrm{s}}{.}5$	$48° \ 9'47\!''\!.0$	23.32 ± 0.09	20.10 ± 0.03	19.40 ± 0.03	18.71 ± 0.03
Object-4	$21^{\mathrm{h}}13^{\mathrm{m}}17\overset{\mathrm{s}}{.}7$	$48° \ 6'43\!''\!.7$	23.73 ± 0.06	20.63 ± 0.03	19.86 ± 0.05	19.28 ± 0.04
Object-5	$21^{\mathrm{h}}13^{\mathrm{m}}12\overset{\mathrm{s}}{.}0$	$48°18' \ 0\!''\!.6$	$\cdots$	21.89 ± 0.07	20.53 ± 0.05	19.81 ± 0.06
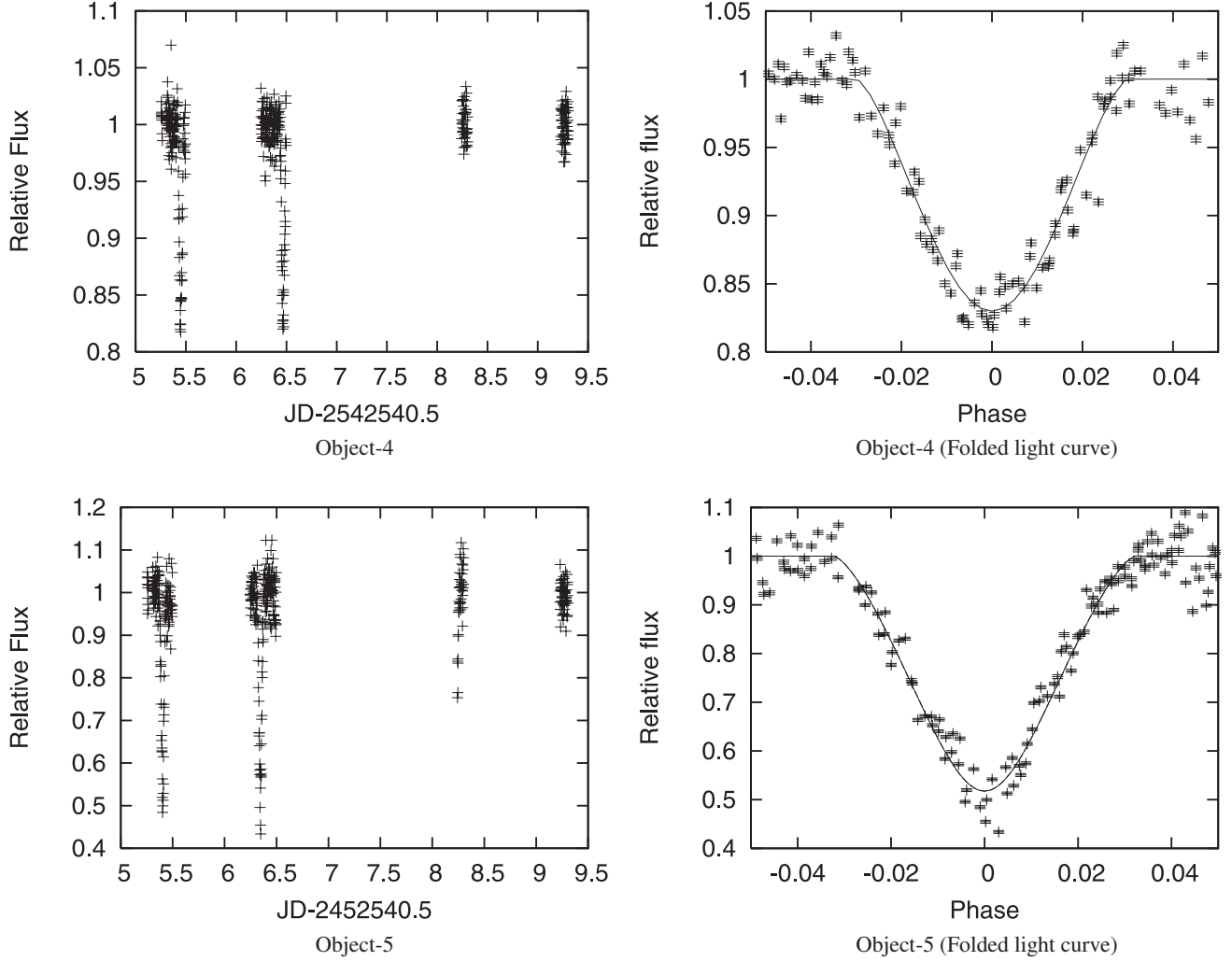
Fig. 6. *Left*: Light curves for the double transiting candidates during this observing run. *Right*: Folded light curves. The best-fit light curve models are based on Ohta, Taruya, and Suto (2005). We assume a K5 dwarf radius for Object-4. For Object-5 whose spectral type is unknown, we tentatively assume $1\,R_\odot$ for its parent star.

the distance is estimated as 0.3–1.2 kpc for M0/M5 dwarf. The companion radius is $(0.6–1.3)\,R_{\rm J}$, the orbital period 2.1–6.9 d, the semi-major axis 0.02–0.03 AU, and the inclination 86°–89°. This set of parameters is consistent with a Jupiter-size companion.

4.2. *Object 2*

Multicolor photometry indicates that Object-2 ($i' = 18.50$ AB mag) is likely to be a late K giant, but if it is a giant, the inferred distance of 84 kpc exceeds the Galaxy's size. Moreover, given the observed scatter of objects in figure 2, a dwarf could well be

Table 4.   Estimated parameters for the transiting candidates assuming that they are dwarfs.*

Object	Spectral type	A_V [mag]	ΔF [%]	$t_{\rm T}$ [min]	$t_{\rm F}$ [min]	P [d]	a [AU]	i [°]	Distance [kpc]	Radius [$R_{\rm J}$]
Object-1	G0V/K5V	3.1	3.9 ± 0.8	76–92	0–34	0.3–1.8	0.01–0.02	67–84	1.0–3.0	1.4–2.2
	M0V/M5V	1.1	4.4 ± 0.8	91–111	0	2.1–6.9	0.02–0.03	86–89	0.3–1.2	0.6–1.3
Object-2	K5V/M0V	1.1	4.9 ± 0.5	101–106	23–34	1.5–2.5	0.02–0.03	84–86	1.3–2.3	1.3–1.6
Object-3-A	K0V/M2V	1.4	3.2 ± 0.4	106–111	0–39	1.7–5.6	0.03–0.05	83–88	1.2–3.0	0.9–1.5
Object-4	K5V/M0V	1.6	17.0 ± 1.6	86–93	0	1.018	0.02	84	2.3–4.0	2.5–3.0
Object-5	$\cdots$	$\cdots$	48.2 ± 4.1	90	0	0.942	$\cdots$	$\cdots$	$\cdots$	$\cdots$

* Total transit duration and the flat-bottom duration are represented by $t_{\rm T}$ and $t_{\rm F}$, respectively. The uncertainties in $t_{\rm T}$, $t_{\rm F}$, P, a, i, and radius come from the uncertainties of the spectral type.

located at the position of Object-2 in the color–color diagram. Therefore, it is quite possible that Object-2 is a K5/M0 dwarf. Adopting this interpretation, we obtain a distance of 1.3–2.3 kpc, a companion radius of (1.3–1.6) R_J, an orbital period of 1.5–2.5 d, a semi-major axis of 0.02–0.03 AU, and an inclination of 84°–86°.

4.3. Object 3

Object-3 turned out to be a very close double star with a separation of $\sim 0.''6$; their individual fluxes cannot be separated via aperture photometry. We thus reanalyzed Object-3 using PSF photometry. The results are shown in figure 5. We find that Object-3 consists of Object-3-A ($i' = 18.47$ AB mag) and Object-3-B ($i' = 19.40$ AB mag) and that the transit-like feature preferentially appears in Object-3-A.

Multicolor photometry suggests that Object-3-A is a K0/M2 star. We estimated the depth, the transit durations, and the flat-bottom durations from the model light curves plotted in figure 4, since the light curve for Object-3-A from the PSF photometry is noisier and still may not completely free from flux contamination of Object-3-B. Ascribing the total flux decrement to a companion around Object-3-A, we derived the transit depth of Object-3-A as being 3.2% using the mean brightness ratio of Object-3-A and Object-3-B from the PSF photometry.

Assuming that a companion orbits around a K0/M2 dwarf, the distance is 1.2–3.0 kpc and the companion radius is (0.9–1.5) R_J; the orbital period is 1.7–5.6 d, the semi-major axis is 0.03–0.05 AU, and the inclination is 83°–88°.

4.4. Object 4

Object-4 ($i' = 19.86$ AB mag) exhibited double transits of a fairly large depth of $17.0 \pm 1.6\%$. The PDM method suggests an orbital period of 1.018 d, and multicolor photometry indicates that Object-4 is a K5/M0 star. The light curve has a transit duration of 86–93 min and does not show a flat-bottomed shape. Assuming that Object-4 is a K5/M0 dwarf, the distance is 2.3–4.0 kpc. For a circular-orbiting companion, the semi-major axis is 0.02 AU, the inclination is 84°, the companion radius is (2.5–3.0) R_J. Thus, the companion of Object-4 is likely to be a late M dwarf. Since the observing run did not cover the full phase, we were unable to detect a secondary eclipse.

4.5. Object 5

Object-5 ($i' = 20.53$ AB mag) also exhibited double transits of a significant depth of $48.2 \pm 4.2\%$. Because of the large depth, Object-5 is likely to be an eclipsing binary system with an orbital period of 0.942 d. Because Object-5 is very faint, we were not able to identify Object-5 in our B-band data. Thus, we could not determine its spectral type and the other parameters.

5.   Summary

We carried out a photometric search for transiting extrasolar planets using Subaru Suprime-Cam. Out of about 100000 stars monitored, we obtained 7700 light curves with photometric precision below 1%. This result thus demonstrates that Suprime-Cam indeed has the photometric stability and accuracy required for a transiting planet survey. However, the detection of multiple transits via long observing runs would be hard to achieve due the very large amounts of Subaru time that they would require.

During this observing run, we detected three transiting planetary candidates (around 18.5 mag for i'-band) that exhibit a single full transit-like light curve with a depth of $< 5\%$. Adopting typical parameters for the parent stars from their spectral types, we infer that their orbital elements are consistent with planetary size companions. While a spectroscopic follow-up remains to be done using a future telescope in the 20–30 m class, we would be able to conduct synoptic photometric monitoring using 2 m class ones.

Appendix.   W UMa-like Eclipsing Binary Candidates

We also detected eleven W UMa-like objects with periods of less than 0.4 days. The light curves are shown in figure 7. The observational results are given in tables 5 and 6. In order to determine the distance, we used the color–magnitude relation and period–color relation (Rucinski 1998) for the spectral type between early F and middle K stars. These are written as

$$M_V = -4.44 \log P + 3.02 (B - V) + 0.12, \tag{A1}$$

$$(B - V) = 0.04 \times P^{-2.25}. \tag{A2}$$

Here, M_V is the absolute magnitude and P is the period. Substituting equation (A2) for equation (A1), we could calculate the absolute magnitude without observations for the B-band and V-band. If the spectral type of objects was not between early F and middle K, the distance was estimated by the typical absolute magnitude for the spectral type of the objects.
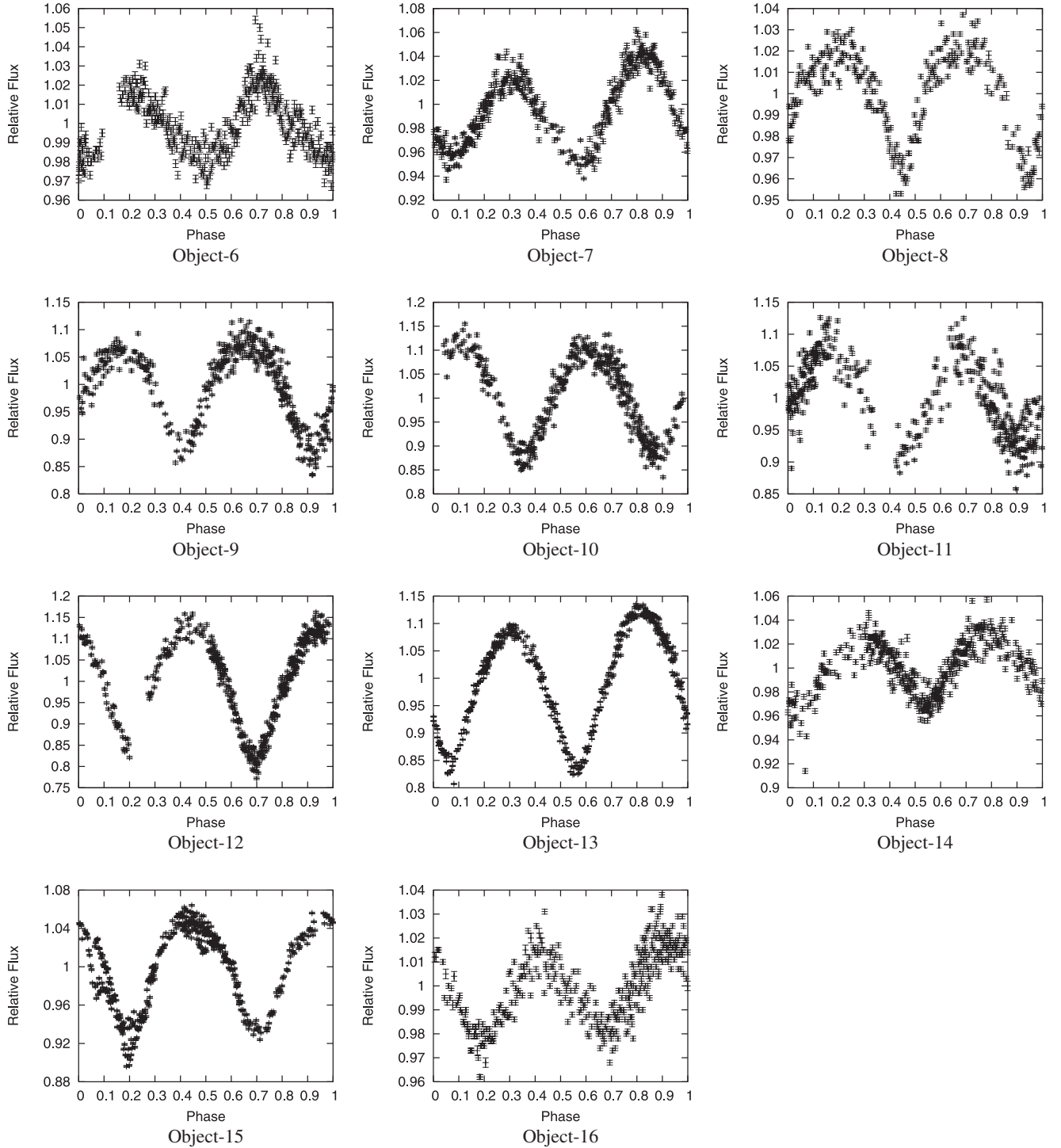
Fig. 7. Light curves of W UMa-like objects.

Object-6: The amplitude is approximately 2%. The period is 0.309 d. Multicolor photometry suggests a K5/M2 star. If Object-6 is a dwarf, the distance is 0.7–1.7 kpc.

Object-7: The primary minimum and the secondary minimum are approximately 5% and 3%, respectively. The period is 0.225 d. Multicolor photometry suggests a K0/M2 star. The distance of 3.1 kpc obtained from equation (A1) and equation (A2).

Object-8: The amplitude is approximately 3%. The period is 0.254 d. Multicolor photometry suggests a F8/K2 or M2/M5 star. If Object-8 is a F8/K2 dwarf, the distance is 1. kpc. In the case of an M2/M5 dwarf, the estimated distance of 0.4–1.1 kpc is obtained from its expected absolute magnitude.

Table 5.   Observed parameters for W UMa-like objects.

Object	RA	Dec	B [mag] (Phase)	R_c [mag] (Phase)	i' [AB mag] (Phase)	z' [AB mag] (Phase)
Object-6	$21^h13^m24^s.1$	$48°29'49''.9$	23.20 ± 0.05 (0.61)	19.66 ± 0.03 (0.79)	18.78 ± 0.10 (0.78)	18.04 ± 0.04 (0.82)
Object-7	$21^h12^m29^s.2$	$48°7'31''.8$	21.83 ± 0.03 (0.56)	19.28 ± 0.03 (0.94)	19.08 ± 0.06 (0.43)	18.65 ± 0.05 (0.98)
Object-8	$21^h11^m4^s.9$	$48°8'3''.6$	22.54 ± 0.04 (0.35)	19.53 ± 0.03 (0.22)	18.95 ± 0.06 (0.61)	18.18 ± 0.05 (0.26)
Object-9	$21^h12^m1^s.0$	$48°17'29''.2$	24.33 ± 0.13 (0.69)	21.45 ± 0.04 (0.48)	20.48 ± 0.03 (0.17)	19.83 ± 0.03 (0.52)
Object-10	$21^h10^m33^s.1$	$48°15'20''.7$	24.40 ± 0.09 (0.76)	20.86 ± 0.03 (0.61)	20.38 ± 0.06 (0.64)	19.39 ± 0.05 (0.88)
Object-11	$21^h10^m31^s.9$	$48°8'18''.5$	23.91 ± 0.07 (0.95)	20.83 ± 0.04 (0.70)	20.21 ± 0.06 (0.73)	19.39 ± 0.05 (0.34)
Object-12	$21^h10^m27^s.8$	$48°14'30''.8$	24.34 ± 0.10 (0.75)	20.81 ± 0.03 (0.47)	20.39 ± 0.06 (0.50)	19.35 ± 0.06 (0.20)
Object-13	$21^h11^m23^s.9$	$48°11'43''.7$	22.10 ± 0.05 (0.06)	19.34 ± 0.03 (0.66)	19.28 ± 0.06 (0.09)	18.53 ± 0.06 (0.69)
Object-14	$21^h11^m37^s.4$	$48°21'45''.5$	22.95 ± 0.05 (0.75)	19.93 ± 0.03 (0.47)	19.40 ± 0.05 (0.50)	18.64 ± 0.03 (0.20)
Object-15	$21^h10^m50^s.9$	$48°32'18.5$	21.39 ± 0.03 (0.34)	18.54 ± 0.03 (0.02)	18.19 ± 0.05 (0.93)	17.55 ± 0.03 (0.04)
Object-16	$21^h10^m21^s.1$	$48°22'20''.1$	21.48 ± 0.04 (0.70)	19.04 ± 0.03 (0.61)	18.73 ± 0.05 (0.85)	18.21 ± 0.04 (0.65)

Table 6.   Estimated parameters for W UMa-like objects assuming that they are dwarfs.

Object	Spectral type	Period [d]	Amplitude Primary | Secondary [%]	Distance [kpc]
Object-6	K5V/M2V	0.309	2	0.7–1.7
Object-7	K0V/M2V	0.225	5 | 3	3.1
Object-8	F8V/K2V or M2V/M5V	0.254	3	1.6 or 0.4–1.1
Object-9	G5V/K5V or M2V/M5V	0.260	12 | 7	6.7 or 1.3–3.3
Object-10	F5V/K2V or M2V/M5V	0.346	10	5.4 or 0.5–1.3
Object-11	F8V/K2V or M2V/M5V	0.358	10	9.3 or 0.7–1.9
Object-12	F0V/G8V	0.362	18 | 15	5.1
Object-13	F0V/K0V	0.270	15 | 13	2.1
Object-14	G5V/K5V or M0V/M5V	0.259	3	2.8 or 0.4–1.6
Object-15	G0V/K7V or M0V/M5V	0.368	8 | 6	5.8 or 0.3–1.2
Object-16	G5V/K5V or M0V/M5V	0.252	2	2.5 or 0.5–1.9

   Object-9: The primary and secondary minimums are approximately 12% and 7%, respectively. The period is 0.260 d. Multicolor photometry suggests a G5/K5 or an M2/M5 star. If Object-9 is a G5/K5 dwarf, the distance is 6.7 kpc. In the case of an M2/M5 dwarf, the estimated distance is 1.3–3.3 kpc.
   Object-10: The amplitude is approximately 10%. The period is 0.346 d. Multicolor photometry suggests a F5/K2 or an M2/M5 star. If Object-10 is a F5/K2 dwarf, the distance is 5.4 kpc. In the case of an M2/M5 dwarf, the estimated distance is 0.5–1.3 kpc.
   Object-11: The amplitude is approximately 10%. The period is 0.358 d. Multicolor photometry suggests a F8/K2 or M2/M5 star. If Object-11 is a F8/K2 dwarf, the distance is 9.3 kpc. In the case of an M2/M5 dwarf, the estimated distance is 0.7–1.9 kpc.
   Object-12: The primary and secondary minimums are approximately 18% and 15%, respectively. The period is 0.362 d. Multicolor photometry suggests a F0/G8 star. If Object-12 is a dwarf, the distance is 5.1 kpc.

Object-13: The primary and secondary minimums are approximately 15% and 13%, respectively. The period is 0.270 d. Multicolor photometry suggests a F0/K0 star. If Object-13 is a dwarf, the distance is 2.1 kpc.

Object-14: The amplitude is approximately 3%. The period is 0.259 d. Multicolor photometry suggests a G5/K5 or an M0/M5 star. If Object-14 is a G5/K5 dwarf, the distance is 2.8 kpc. In the case of an M0/M5 dwarf, the estimated distance is 0.4–1.6 kpc.

Object-15: The primary and secondary minimums are approximately 8% and 6%, respectively. The period is 0.368 d. Multicolor photometry suggests a G0/M5 star. If Object-15 is a G0/K7 dwarf, the distance is 5.8 kpc. In the case of an M0/M5 dwarf, the estimated distance is 0.3–1.2 kpc.

Object-16: The amplitude is approximately 2%. The period is 0.252 d. Multicolor photometry suggests a G5/K5 star or an M0/M5 star. If Object-16 is a G5/K5 dwarf, the distance is 2.5 kpc. In the case of an M0/M5 dwarf, the estimated distance is 0.5–1.9 kpc.

References

Abe, F., et al. 2005, MNRAS, 364, 325

Alonso, R., et al. 2004, ApJ, 613, L153

Bakos, G., Noyes, R. W., Kovács, G., Stanek, K. Z., Sasselov, D. D., & Domsa, I. 2004, PASP, 116, 266

Basri, G., Borucki, W. J., & Koch, D. 2005, New Astron. Rev., 49, 478

Bessell, M. S. 1990, PASP, 102, 1181

Bordé, P., Rouan, D., & Léger, A. 2003, A&A, 405, 1137

Borucki, W. J., Caldwell, D., Koch, D. G., Webster, L. D., Jenkins, J. M., Ninkov, Z., & Showen, R. 2001, PASP, 113, 439

Bouchy, F., et al. 2005a, A&A, 444, L15

Bouchy, F., Pont, F., Melo, C., Santos, N. C., Mayor, M., Queloz, D., & Udry, S. 2005b, A&A, 431, 1105

Bouchy, F., Pont, F., Santos, N. C., Melo, C., Mayor, M., Queloz, D., & Udry, S. 2004, A&A, 421, L13

Burke, C. J., Gaudi, B. S., DePoy, D. L., & Pogge, R. W. 2006, AJ, 132, 210

Charbonneau, D., Brown, T. M., Latham, D. W., & Mayor, M. 2000, ApJ, 529, L45

Christian, D. J., et al. 2004, in Proc. of the 13th Cool Stars Workshop, ed. F. Favata (ESA-SP)

Cox, A. N. 2000, Allen's Astrophysical Quantities, 4th ed. (New York: AIP), 389

Deeg, H. J., Alonso, R., Belmonte, J. A., Alsubai, K., Horne, K., & Doyle, L. 2004, PASP, 116, 985

Dreizler, S., Rauch, T., Hauschildt, P., Schuh, S. L., Kley, W., & Werner, K. 2002, A&A, 391, L17

Fukugita, M., Ichikawa, T., Gunn, J. E., Doi, M., Shimasaku, K., & Schneider, D. P. 1996, AJ, 111, 1748

Gaudi, B. S., Seager, S., & Mallén-Ornelas, G. 2005, ApJ, 623, 472

Gould, A., Dorsher, S., Gaudi, B. S., & Udalski, A. 2006, Acta Astron., 56, 1

Hood, B., et al. 2005, MNRAS, 360, 791

Konacki, M., et al. 2004, ApJ, 609, L37

Konacki, M., Torres, G., Sasselov, D. D., & Jha, S. 2003a, Nature, 421, 507

Konacki, M., Torres, G., Sasselov, D. D., & Jha, S. 2003b, ApJ, 597, 1076

Konacki, M., Torres, G., Sasselov, D. D., & Jha, S. 2005, ApJ, 624, 372

Lomb, N. R. 1976, Ap&SS, 39, 447

Mallén-Ornelas, G., Seager, S., Yee, H. K. C., Minniti, D., Gladders, M. D., Mallén-Fullerton, G. M., & Brown, T. M. 2003, ApJ, 582, 1123

Mayor, M., & Queloz, D. 1995, Nature, 378, 355

McCullough, P. R., Stys, J. E., Valenti, J. A., Fleming, S. W., Janes, K. A., & Heasley, J. N. 2005, PASP, 117, 783

Miyazaki, S., et al. 2002, PASJ, 54, 833

Mochejska, B. J., et al. 2005, AJ, 129, 2856

Mochejska, B. J., et al. 2006, AJ, 131, 1090

Moutou, C., Pont, F., Bouchy, F., & Mayor, M. 2004, A&A, 424, L31

Ohta, Y., Taruya, A., & Suto, Y. 2005, ApJ, 622, 1118

Oke, J. B. 1990, AJ, 99, 1621

Ouchi, M., et al. 2004, ApJ, 611, 660

Pepper, J., Gould, A., & DePoy, D. L. 2004, in The Search for Other Worlds, ed. S. S. Holt & D. Deming (Melville, NY: AIP), 185

Pont, F., Bouchy, F., Queloz, D., Santos, N. C., Melo, C., Mayor, M., & Udry, S. 2004, A&A, 426, L15

Press, W. H., Teukolsky, S. A., Vetterling, W. T., & Flannery, B. P. 1992, in Numerical Recipes in FORTRAN (New York: Cambridge University Press), 569

Rauer, H., Eislöffel, J., Erikson, A., Guenther, E., Hatzes, A. P., Michaelis, H., & Voss, H. 2004, PASP, 116, 38

Rucinski, S. M. 1998, AJ, 116, 2998

Sato, B., et al. 2005, ApJ, 633, 465

Seager, S., & Mallén-Ornelas, G. 2003, ApJ, 585, 1038

Stellingwerf, R. F. 1978, ApJ, 224, 953

Torres, G., Konacki, M., Sasselov, D. D., & Jha, S. 2004, ApJ, 609, 1071

Torres, G., Konacki, M., Sasselov, D. D., & Jha, S. 2005, ApJ, 619, 558

Udalski, A., et al. 2002a, Acta Astron., 52, 1

Udalski, A., Pietrzyński, G., Szymański, M., Kubiak, M., Żebruń, K., Soszyński, I., Szewczyk, O., & Wyrzykowski, Ł. 2003, Acta Astron., 53, 133

Udalski, A., Szewczyk, O., Żebruń, K., Pietrzyński, G., Szymański, M., Kubiak, M., Soszyński, I., & Wyrzykowski, Ł. 2002c, Acta Astron., 52, 317

Udalski, A., Szymański, M., Kubiak, M., Pietrzyński, G., Soszyński, I., Żebruń, K., Szewczyk, O., & Wyrzykowski, Ł. 2004, Acta Astron., 54, 313

Udalski, A., Żebruń, K., Szymański, M., Kubiak, M., Soszyński, I., Szewczyk, O., Wyrzykowski, Ł., & Pietrzyński, G. 2002b, Acta Astron., 52, 115

von Braun, K., Lee, B. L., Seager, S., Yee, H. K. C., Mallén-Ornelas, G., & Gladders, M. D. 2005, PASP, 117, 141

Yagi, M., Kashikawa, N., Sekiguchi, M., Doi, M., Yasuda, N., Shimasaku, K., & Okamura, S. 2002, AJ, 123, 66